SHORT COMMUNICATION

ARCH PHARM DPhG
Archiv der Pharmazie

BC-11 is a covalent TMPRSS2 fragment inhibitor that impedes SARS-CoV-2 host cell entry

Aurélien F. A. Moumbock[1] 🟢 | **Hoai T. T. Tran[2]** | **Evelyn Lamy[2]** | **Stefan Günther[1]** 🟢

[1]Faculty of Chemistry and Pharmacy, Institute of Pharmaceutical Sciences, Albert-Ludwigs-Universität Freiburg, Freiburg, Germany

[2]Molecular Preventive Medicine, Faculty of Medicine, University Medical Center, Albert-Ludwigs-Universität Freiburg, Freiburg, Germany

Correspondence
Stefan Günther, Faculty of Chemistry and Pharmacy, Albert-Ludwigs-Universität Freiburg, Institute of Pharmaceutical Sciences, Hermann-Herder-Str. 9, Freiburg 79104, Germany.
Email: stefan.guenther@pharmazie.uni-freiburg.de

Abstract
Host cell entry of severe acute respiratory syndrome coronavirus 2 (SARS-CoV-2) is facilitated via priming of its spike glycoprotein by the human transmembrane protease serine 2 (TMPRSS2). Although camostat and nafamostat are two highly potent covalent TMPRSS2 inhibitors, they nevertheless did not hold promise in COVID-19 clinical trials, presumably due to their short plasma half-lives. Herein, we report an integrative chemogenomics approach based on computational modeling and in vitro enzymatic assays, for repurposing serine-targeted covalent inhibitors. This led to the identification of BC-11 as a covalent TMPRSS2 inhibitor displaying a unique selectivity profile for serine proteases, ascribable to its boronic acid warhead. BC-11 showed modest inhibition of SARS-CoV-2 (omicron variant) spike pseudo-typed particles in a cell-based entry assay, and a combination of BC-11 and AHN 1-055 (a spike glycoprotein inhibitor) demonstrated better viral entry inhibition than either compound alone. Given its low molecular weight and good activity against TMPRSS2, BC-11 qualifies as a good starting point for further structural optimizations.

KEYWORDS
BC-11, CovPDB, SARS-CoV-2 cell entry, targeted covalent inhibitor, TMPRSS2

1 | INTRODUCTION

The coronavirus disease 2019 (COVID-19) pandemic emerged from an outbreak in Wuhan (China) in late December 2019 and was declared by the World Health Organization as a public health emergency of international concern on 11th March 2020.[1] As of 13th March 2022, COVID-19 has since led to over 455 million confirmed infection cases for more than 6 million deaths world-wide.[2] Its causative pathogen, the severe acute respiratory syndrome coronavirus 2 (SARS-CoV-2), is a positive-sense single-stranded RNA virus of the Betacoronavirus genus to which also belong the pathogens SARS-CoV-1 and Middle East respiratory

syndrome coronavirus (MERS-CoV), responsible for the SARS and MERS outbreaks in 2003 and 2012, respectively.[3]

SARS-CoV-2 infects host cells through the tight binding of its spike glycoprotein to the surface-exposed angiotensin-converting enzyme 2 (ACE2) of vertebrates, followed by host cell entry (Figure 1). Host cell viral entry can occur: primarily via a fast "early" pH-independent pathway, wherein the fusion of viral and host cell membranes is facilitated by the priming of the spike protein at the S1/S2 and S2' site by the human transmembrane protease serine 2 (TMPRSS2); or secondarily via a slow "late" pH-dependent pathway involving endocytosis, wherein cathepsin L (CTSL) primes the spike protein at the S1/S2 site.[4,5] Moreover, priming of the spike protein
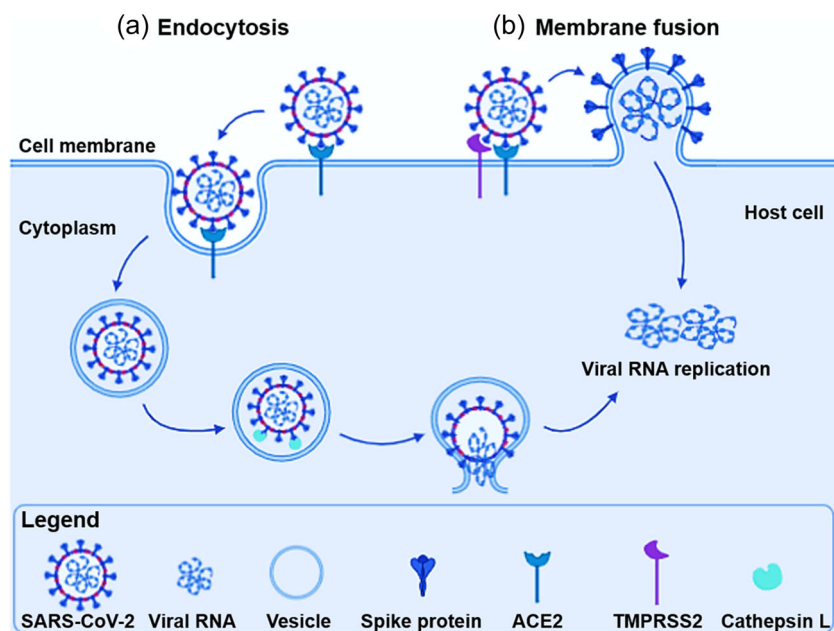
FIGURE 1 Severe acute respiratory syndrome coronavirus 2 host cell entry mechanism. Image credit: Pislar et al.[5]. Copyright 2020, PLOS, licensed under CC BY 4.0 (http://creativecommons.org/licenses/by/4.0/).

at the S1/S2 site can also be achieved by the human furin endoprotease in the early pathway.[6] Although several vaccines and monoclonal antibodies targeting the spike protein have been developed and approved by regulatory agencies around the globe, these biologics are susceptible to resistance due to the inherently high mutation rate of SARS-CoV-2, predominantly on its spike protein.[7] Conversely, the functionally redundant TMPRSS2 (no phenotype observed in knockout mice) is less susceptible to mutations,[8] thus serving as a suitable target for viral entry inhibitors, that is, indirect-acting antivirals. Low expression levels of TMPRSS2 in infants and children correlate with relatively low infection rates in this age group compared to adults.[9] Adults with Down syndrome, on the other hand, typically overexpress TMPRSS2 and this correlates with a much higher risk of mortality from COVID-19 than people without Down syndrome.[10]

The trypsin-like serine protease domain of TMPRSS2 is characterized by its S4-S3-S2-S1-S1′-S2′-S3′-S4′ subsites with a conserved Ser441–His296–Asp345 catalytic triad in its active site (S1–S1′).[11] Camostat and nafamostat are two highly potent TMPRSS2 inhibitors that form an irreversible covalent bond with the nucleophilic Ser441, and they have been established as efficacious SARS-CoV-2 host viral entry inhibitors.[12,13] However, they did not hold promise in COVID-19 clinical trials,[14,15] presumably due to their short plasma half-lives of approximately an hour or less.[16,17] Therefore, there is a dire need to identify novel and potent targeted covalent inhibitors (TCIs) of TMPRSS2 to impede host cell viral entry. For an overview of serine-TCIs used in the treatment of lung inflammatory diseases, the reader is referred to a recently published comprehensive review.[18] To considerably decrease the amount of time and resources needed to identify potential TCIs of TMPRSS2, computational methods such as molecular docking can be applied for drug repurposing.[19]

In the present study, we describe an efficient computational drug repurposing strategy used in conjunction with enzymatic and cell-based functional assays to identify TMPRSS2 acting as SARS-CoV-2 entry inhibitors.

2 | RESULTS AND DISCUSSION

Starting from the recently disclosed 1.95 Å X-ray crystal structure of TMPRSS2 ectodomain in complex with nafamostat (PDB ID: 7 meq),[11] we carried out a covalent docking-based virtual screening with the CovDock[20] algorithm and a TCI subset annotated in the CovPDB[21] (http://www.pharmbioinf.uni-freiburg.de/covpdb), a database we recently developed. Briefly, CovPDB contains 462 TCIs which covalently modify a nucleophilic serine residue of their target proteins. Among these serine TCIs (representing 38 different warheads), beta-lactams were excluded and not all the remaining TCIs are commercially available. Hence, only boronic acids, ketones, aldehydes, halomethyl carbonyls, and nitriles were retained for virtual screening, amounting to a total of 215 TCIs. Three different predefined SMARTS-based CovDock reactions were used for covalent docking, namely: (i) boronic acid addition (for boronic acids); (ii) nucleophilic addition to a double bond (for aldehydes, ketones, and halomethyl carbonyls); and (iii) nucleophilic addition to a triple bond (for nitriles). The predicted covalent protein-ligand complexes were visually inspected for shape complementarity and (non)covalent interactions between the binding partners. On this basis, seven top-ranked candidate compounds with a good fit binding mode were selected from all warhead groups for experimental evaluation (Figure 2).

Candidate compounds were tested at a maximum concentration of 10 μM in an in vitro TMPRSS2 enzymatic assay, with camostat as
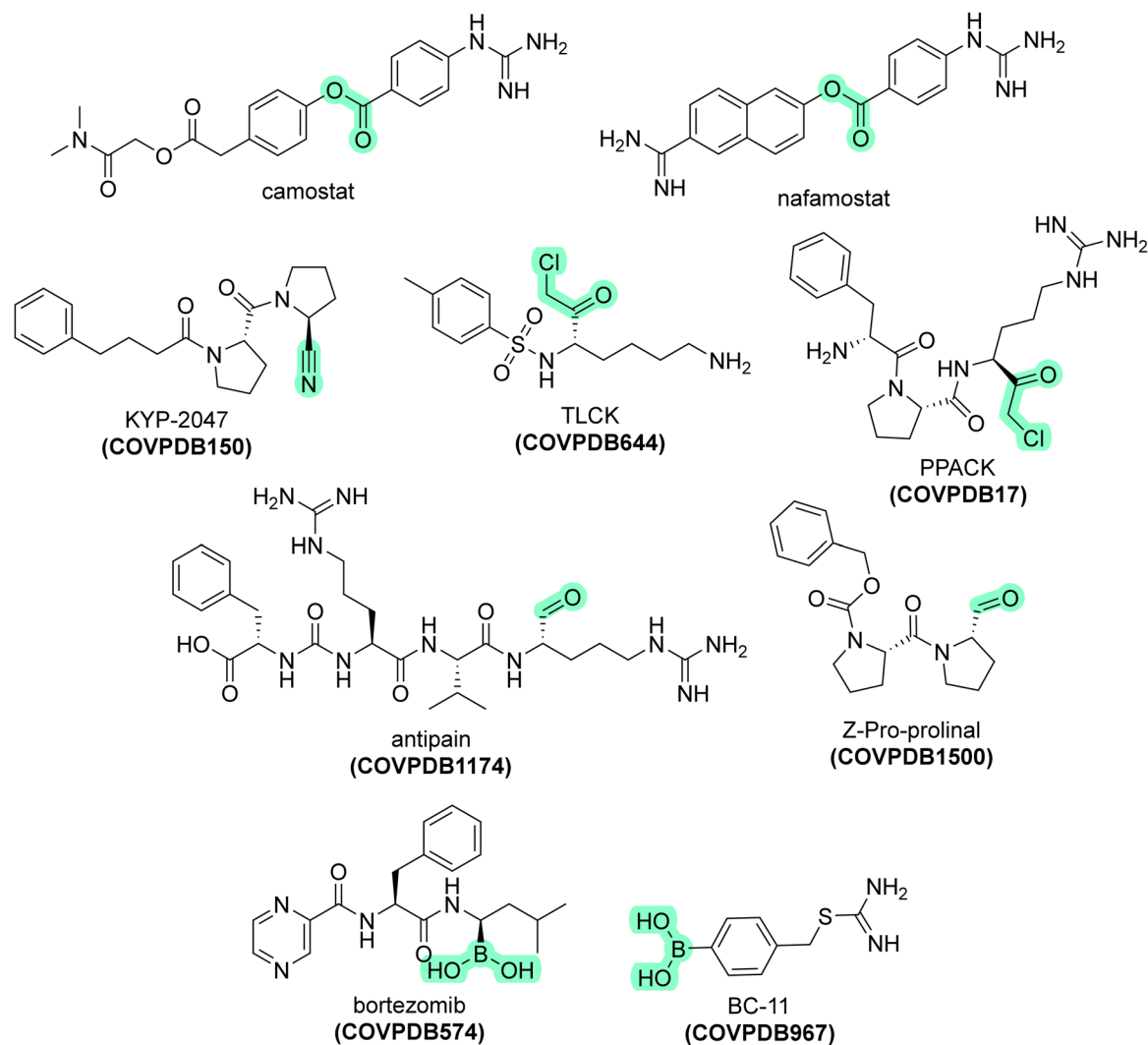
FIGURE 2   Chemical structures of two known transmembrane protease serine 2 (TMPRSS2) inhibitors, along with those of the top-7 ranked CovPDB virtual screening hits. Reactive electrophilic warheads are highlighted in green.

a positive control. Half-maximal inhibitory concentration (IC_{50}) values were determined by a 3-fold serial dilution protocol in a 10-dose triplet format. Three out of seven candidate compounds were identified as hits: the chloromethyl ketone D-Phe-L-Pro-L-Arg chloromethyl ketone (PPACK), the aldehyde antipain, and the boronic acid BC-11, with IC_{50} values of 3.95, 152, and 1440 nM, respectively (Figure 3a); camostat displayed an IC_{50} value of 0.83 nM. We next assessed the selectivity of the identified TMPRSS2 hits at a maximum concentration of 10 µM (singlet format) against three other key human proteases implicated in SARS-CoV-2 pathogenesis, including the cysteine proteases CATSL and CATSB, and the serine protease furin. Against CATSL, antipain (IC_{50} = 2.74 nM) was found to be more potent than both PPACK (IC_{50} = 19 nM) and the positive control E-64 (IC_{50} = 4 nM), as illustrated in Figure 3b. A similar trend in potency was observed against CATSB (Figure 3c), with antipain (IC_{50} = 24.1 nM) being

more potent than PPACK (IC_{50} = 402 nM), but this time around less potent than E-64 (IC_{50} = 8.83 nM). Only antipain (IC_{50} = 4.17 µM) displaced significant activity against furin, with furin inhibitor I (IC_{50} = 2.18 nM) as positive control (Figure 3d). Interestingly, BC-11 was inactive against all three proteases (furin, CATSB, and CATSL) and owes its selectivity toward serine proteases over cysteine proteases to the thermodynamic instability of the tetrahedral intermediate formed by the nucleophilic attack of a catalytic cysteine residue and its boronic acid warhead.[22] Since TMPRSS2 belongs to the highly conserved type 2 transmembrane serine protease (TTSP) family containing also TMPRSS3-5, hepsin, and enteropeptidase,[23] it cannot be ruled out that BC-11 could also inhibit other TTSP family members. Further optimized molecules should be studied on this aspect.

The trend in potency observed among the identified TMPRSS2 inhibitors can be rationalized by their predicted covalent docking
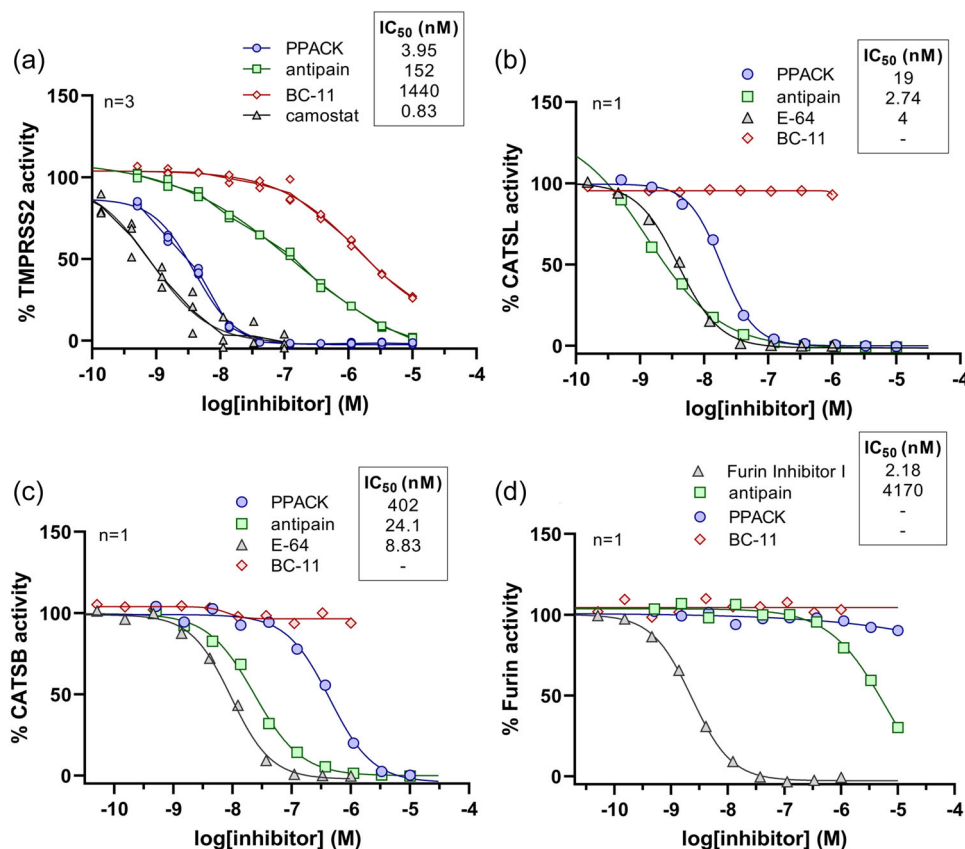
FIGURE 3 Activity data of selected virtual screening candidate compounds against human proteases implicated in severe acute respiratory syndrome coronavirus 2 (SARS-CoV-2) pathogenesis: (a) transmembrane protease serine 2 (TMPRSS2), (b) CATSL, (c) CATSB, and (d) furin.

models in comparison to the X-ray crystal structure of the TMPRSS2–nafamostat complex (PDB ID: 7 meq), all shown in Figure 4. It is worth mentioning that camostat and nafamostat form identical covalent complexes with TMPRSS2. Their mechanism of action involves the nucleophilic attack of their scissile ester bond by Ser441 at the S1' subsite, to form a covalent adduct (Figure 4a). In addition to the covalent bond, the carbonyl of nafamostat is stabilized by H-bonds formed with the backbone NH groups of Ser441 and Gly439, also known as the "oxyanion hole." At the S1 subsite, the guanidinium group of nafamostat engages in an arginine-like manner into a salt bridge/H-bond with Asp435, Ser436, and Gly464. A guanidinium or thiouronium group appears to be primordial for tight binding, as illustrated by the fact that only CovPDB virtual screening hits possessing this functional group displayed $IC_{50} \leq 1\,\mu M$ (Figures 2 and 3). The binding mode of BC-11 (Figure 4b) is akin to that of nafamostat, with the difference that the boronic acid warhead of BC-11 additionally establishes an H-bond with the catalytic His296. However, just as camostat, nafamostat shows higher TMPRSS2 potency than BC-11, due to the relatively slower hydrolysis rate of its acyl–Ser441 bond. For the tetrapeptyl aldehyde antipain (L-Phe-CO-L-Arg-L-Val-L-Arg-H), a reversible hemiacetal is formed

between its aldehyde group and Ser441, stabilized by the oxyanion hole (Figure 4c). Both of its Arg residues address the S1 subsite by forming H-bonds and salt bridges with Asp435 and Glu389. Antipain's Phe residue addresses the S2 subsite by establishing a salt bridge with Lys342 and a π–π stacking with Tryp461. The occupancy of the S2 pocket confers antipain a 2-fold increase in potency over BC-11 (Figure 3). The tripeptidyl chloromethyl ketone PPACK (D-Phe-L-Pro-L-Arg-CH$_2$Cl) adopts a binding mode similar to that of antipain, occupying S1', S1, and S2 subsites (Figure 4d). But at the S1' site, its chloromethyl ketone warhead simultaneously forms a reversible covalent bond with Ser441 as well as an irreversible covalent bond with His296, leading to a 30-fold increase in potency of PPACK over antipain.

We next evaluated the identified TMPRSS2 inhibitors in a SARS-CoV-2 spike (delta/omicron variant) pseudotyped particle entry assay in A549-hACE2-TMPRSS2 cells, which are A549 human lung carcinoma cells overexpressing ACE2 and TMPRSS2, and are highly permissive to SARS-CoV-2 infection.[24] Despite its tighter and irreversible binding to TMPRSS2, PPACK showed weaker SARS-CoV-2 viral entry inhibition of 36% at 50 μM compared to 81% at 100 μM for antipain (Figure 5a), with
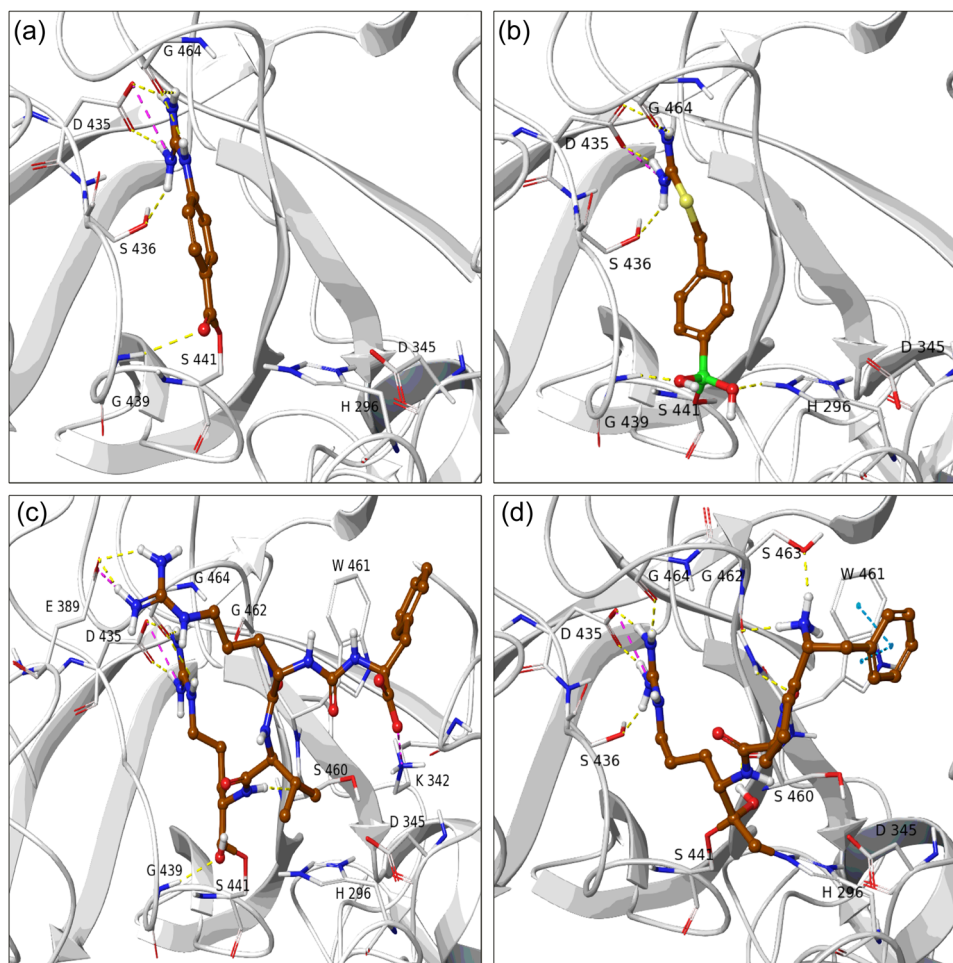
FIGURE 4 Binding poses of targeted covalent inhibitors (TCIs) of transmembrane protease serine 2 (TMPRSS2). (a) Crystallographic pose of nafamostat (PDB ID: 7 meq) in comparison to the docking poses of: (b) BC-11, (c) antipain, and (d) PPACK. The ligand and protein are represented as brown sticks and gray ribbons (and sticks), respectively. Yellow, blue, and purple dotted lines represent H-bond, π–π stacking, and salt bridges, respectively.

camostat as a positive control (97% inhibition at 50 μM). The findings for camostat and antipain are in agreement with those recently reported by Sun et al.[25] Although antipain is a triple TMPRSS2/CATSL/furin inhibitor, its use as a dual pathway SARS-CoV-2 entry inhibitor is limited by its cell impermeability, since CATSL is an endosomal protein.[26] In addition, the acute toxicity of antipain could originate from its broad spectrum serine/cysteine protease inhibition.[27] BC-11 also showed modest inhibition of SARS-CoV-2 entry with a half-maximal effective concentration (EC_{50}) of 66 μM; however, the potency was two orders of magnitude lower than that of camostat, which showed an EC_{50} of 0.98 μM (Figure 5b). The disparity between BC-11's inhibitory activity against TMPRSS2 (IC_{50} = 1.44 μM) and antiviral activity (EC_{50} = 66 μM) can be explained by the fact that SARS-CoV-2 can penetrate host cells via two distinct mechanisms, as mentioned above. Moreover, we observed a similar trend in viral/enzymatic activity for camostat (the positive control), that is,

TMPRSS2 inhibition (IC_{50} = 1.19 nM) and SARS-CoV-2 entry inhibition (EC_{50} = 0.98 μM). Given its low molecular weight and good activity against TMPRSS2, BC-11 qualifies as a good starting point for further structural optimizations. Possible elaboration avenues are to grow the ligand toward the S2 subsite and/or enhance the strength of the boronate–Ser441 bond.

To combat antiviral drug resistance, we hypothesize that BC-11 could be combined with other SARS-CoV-2 entry inhibitors possessing a different mechanism of action. Recently, Hu et al.[28] reported difluorobenztropine (AHN 1-055) as a direct-acting SARS-CoV-2 entry inhibitor that targets the SARS-CoV-2 spike fusion peptide domain. In the cell-based entry assay, we observed that the efficacy of AHN 1-055 (EC_{50} > 50 μM) falls in the same range as that of BC-11 (Figure 5c). To test the hypothesis of a combination therapy, we evaluated a 1:1 mixture of a fixed concentration of BC-11 (25 or 50 μM) with various concentrations of AHN 1-055 (6.25, 12.5, and 25 μM) in a cell-based entry assay.
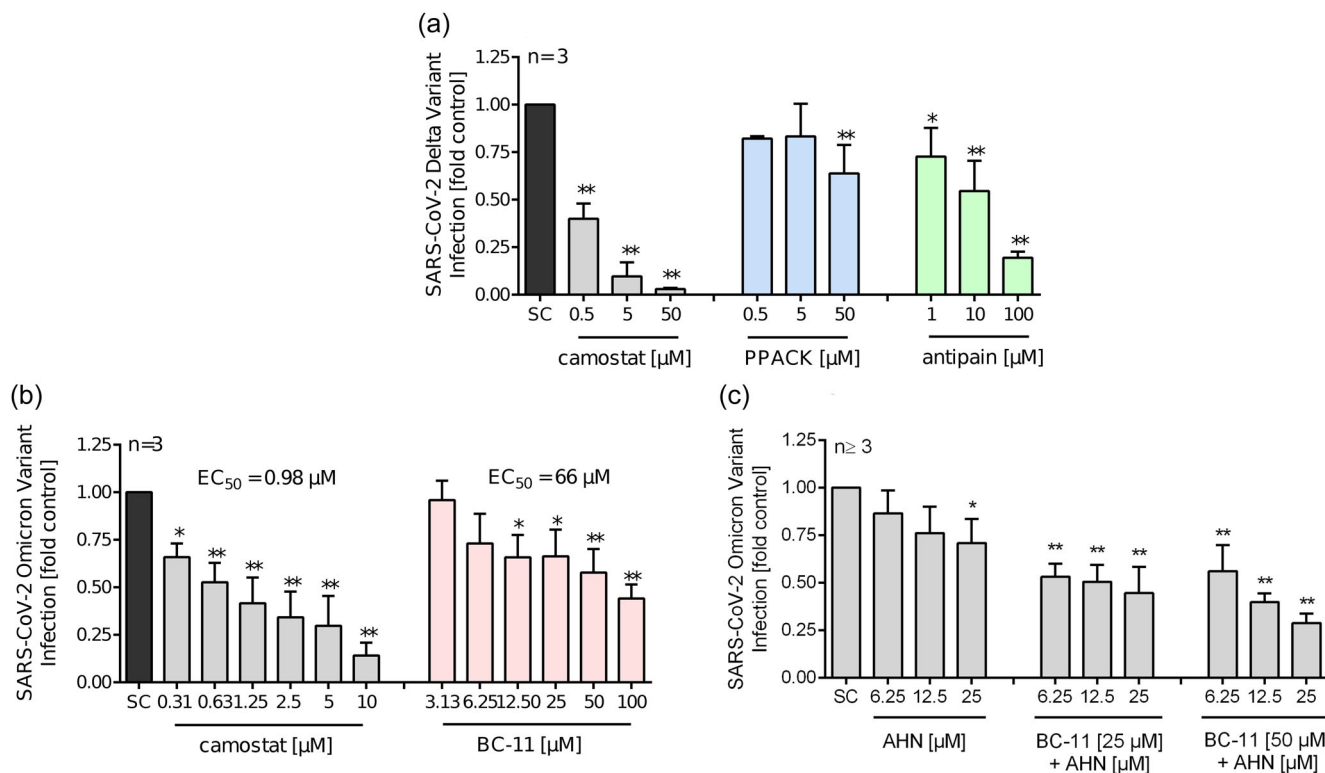
FIGURE 5 Activity data of transmembrane protease serine 2 (TMPRSS2) inhibitors in a severe acute respiratory syndrome coronavirus 2 (SARS-CoV-2) spike pseudotyped particle entry assay in A549-hACE2-TMPRSS2 cells. Data are reported as means + standard deviations of three independent experiments. Significance of difference was calculated relative to the solvent control (SC). p-values < 0.05 (*) were considered statistically significant and <0.01 (**) were considered highly statistically significant.

The combination therapy demonstrated better viral entry inhibition than either compound alone. For instance, at a concentration of 25 µM each, the combination therapy showed 50% inhibition of SARS-CoV-2 viral entry (Figure 5c).

3 | CONCLUSION

In summary, we present an efficient computationally-driven drug repurposing strategy for the identification of TCIs of TMPRSS2. Three hits were identified which displayed micro- to nanomolar inhibition of TMPRSS2 and micromolar entry inhibition of SARS-CoV-2 (delta/omicron variant) pseudotyped particles in lung cell lines. Docking models of their covalent complexes with TMPRSS2 provide structural insights into their mechanism of action. With an interesting serine protease selectivity profile, BC-11 is suggested as a promising candidate for further optimization into a more potent SARS-CoV-2 entry inhibitor. Moreover, a combination of the direct- and indirect-acting antivirals (BC-11 and AHN 1-055) demonstrated better viral entry inhibition than either compound alone. The described integrative chemogenomics approach, based on computational modeling and biochemical assays, appears to be suitable for repurposing TCIs annotated in the CovPDB database to covalently address any protein target possessing a nucleophilic residue.

4 | EXPERIMENTAL

4.1 | Computational modeling

4.1.1 | Protein preparation

Modeling studies were performed with the programs of the Schrödinger Small-Molecule Drug Discovery Suite 2021-1 (Schrödinger LLC). The 1.95 Å X-ray crystal structure of TMPRSS2 ectodomain in complex with nafamostat (PDB ID: 7 meq) was downloaded from the PDB[29] (https://www.rcsb.org/) and prepared with the Protein PrepWizard.[30] This involves adding missing hydrogen atoms, adjusting the ionization state of polar amino acids at neutral pH, while meanwhile adjusting bond orders and formal charges of the ligand, optimizing the H-bond network of the protein-ligand complex, and, finally, energetically minimizing the complex using the OPLS4[31] force field.

4.1.2 | Ligand preparation

The CovPDB[21] database (http://www.pharmbioinf.uni-freiburg.de/covpdb) was queried for serine TCIs. A list of 462 ligands was retrieved and downloaded as a CSV file. The CSV file was modified in such a way that the SMILES and ligand ID columns appeared as the first and second

columns, respectively; meanwhile, other columns were discarded. The 3D SDF file of all CovPDB ligands was equally downloaded from the CovPDB and the 462 serine TCIs were filtered out with the generated CSV file with the "Compare Ligand Files" option of Maestro (Schrödinger LLC). Next, TCIs containing boronic acid, ketone, aldehyde, halomethyl carbonyl, and nitrile warhead were selected with Ligfilter (Schrödinger LLC), amounting to a total of 215 TCIs. Finally, the ligands were prepared with LigPrep (Schrödinger LLC), a step involving the generation of ionization and tautomeric states at pH 7.4 and the geometric optimization of ligand structures using the OPLS4[31] force field.

4.1.3 | Covalent docking

This was performed with CovDock[20] in virtual screening mode. Starting from the prepared TMPRSS2-nafamostat complex, the geometric center of the bound ligand was considered as the docking grid centroid and Ser441 was selected as the reactive residue for covalent attachment. Three different predefined SMARTS-based CovDock reactions were used for covalent docking, namely: (i) boronic acid addition (for boronic acids); (ii) nucleophilic addition to a double bond (for aldehydes, ketones, and halomethyl carbonyls); and (iii) nucleophilic addition to a triple bond (for nitriles). The predicted covalent protein-ligand complexes were visually inspected for shape complementarity and (non)covalent interactions between the binding partners. The top-ranked hits with a good fit binding mode were redocked with CovDock in lead optimization mode, which is more robust but computationally demanding.

4.2 | Pharmacology

4.2.1 | Enzymatic assays

The compounds: PPACK (cat. #15160), TCLK (cat. #13074), antipain hydrochloride (cat. #26705), camostat mesylate (cat. #16018), and bortezomib (cat. #10008822), were purchased from Cayman; KYP-2047 (cat. #SML0208) and Z-Pro-prolinal (cat. #SML0205) from Sigma-Aldrich; AHN 1-055 hydrochloride (cat. #HY-101315) from MedChem-Tronica; and BC-11 hydrobromide (cat. #A4444) from Apexbio Technology LLC. Enzymatic (TMPRSS2, CATSL, CATSB, and furin) assays were carried out on a pay-per-service basis at Reaction Biology

Corporation. Briefly, test compounds were tested in a 10-dose IC_{50} triplet format (TMPRSS2) and singlet format (CATSL, CATSB, and furin) with threefold serial dilution starting at 10 μM. Enzymatic assays were performed using a fluorogenic peptide substrate (Table 1). A fluorescence signal is generated upon peptide cleavage, which is quantified for the determination of protease activity. To a well plate was dispensed a protease diluted in an assay buffer, then added the test compound (in DMSO) using an ECHO 550 acoustic dispenser (LabCyte). After 20 min of incubation at room temperature, the substrate was added to initiate the reaction. Fluorescence was measured on EnVision microplate reader (PerkinElmer, USA) with an excitation at 355 nm and emission at 460 nm, in time intervals of 5 min for a total of 2 h. The initial linear portion of slope (signal/time) was analyzed with Excel (Microsoft Corp.) and curve fits were performed with GraphPad Prism 9.3.1.

The InChI codes of the investigated compounds, together with some biological activity data, are provided as Supporting Information.

4.2.2 | Cell cultures

The one-step luciferase assay system, the SARS-CoV-2 spike (B.1.617.2 delta variant), and (B.1.1.529, omicron variant) pseudotyped lentiviral particles (Luc reporter) were purchased from Biomol (Hamburg, Germany) with cat. #60690, #78215, and #78348, respectively. A549-hACE2-TMPRSS2 cells were purchased from InvivoGen SAS (Toulouse Cedex 4, France) and cultured in DMEM, 4.5 g/L glucose supplemented with 10% heat-inactivated FBS, 100 U/ml penicillin/streptomycin, 100 μg/ml normocin, 0.5 μg/ml puromycin, and 300 μg/ml hygromycin, at 37°C, in a humidified incubator with 5% CO_2, according to the manufacturer's instructions.

4.2.3 | SARS-CoV-2 spike pseudotyped particle entry assay

Transduction of A549-hACE2-TMPRSS2 cells was performed as previously described.[24] Briefly, A549-hACE2-TMPRSS2 cells (1×10^5 cells/cm^2) were seeded into 96-well plates for 8 h. Cells were then pretreated with a test compound or combination therapy for 2 h before transduction with 7500 TU/ml SARS-CoV-2 spike delta (B.1.617.2) or omicron (B.1.1.529) variant for 24 h in DMEM medium

TABLE 1 Reagents for the enzymatic assays

Protease name and source	Substrate name and concentration	Buffer	Control inhibitor
CATSB (human liver)	Z-FR-AMC (10 μM)	25 mM MES pH 6, 50 mM NaCl, 0.005% Brij35, 5 mM DTT	E64
CATSL (human liver)	Z-FR-AMC (10 μM)	400 mM NaAcetate pH 5.5, 4 mM EDTA, 8 mM DTT	E64
Furin (human recombinant aa108–715)	pERTKR-AMC (5 μM)	100 mM Tris-HCl, pH 7.5, 1 mM CaCl2, 0.5% TX-100, 1 mM DTT	Furin I inhibitor
TMPRSS2 (human recombinant)	Boc-Gln-Ala-Arg-AMC (25 μM)	50 mM Tris-HCl, pH 8, 150 mM NaCl, 0.005% Brij35	Camostat mesylate

containing 10% heat-inactivated FBS. Thereafter, the medium was replaced by fresh medium, and cells were post-incubated for 48 h. Luminescence was detected within 1 h using the one-step luciferase assay system (BPS Bioscience, cat. #60690) following the manufacturer's protocol using a multiplate reader from Tecan (Tecan Group Ltd.). Results were analyzed with GraphPad Prism 9.3.1. Data are reported as means + standard deviations of three independent experiments. The significance of difference was determined relative to solvent control (0.1% DMSO) by the one-way analysis of variance test followed by Bonferroni correction. p-values < 0.05 (*) were considered statistically significant and <0.01 (**) were considered highly statistically significant.

CONFLICTS OF INTEREST

The authors declare no conflicts of interest.

ORCID

Aurélien F. A. Moumbock http://orcid.org/0000-0002-6034-2016
Stefan Günther http://orcid.org/0000-0003-3744-189X

REFERENCES

[1] N. Zhu, D. Zhang, W. Wang, X. Li, B. Yang, J. Song, X. Zhao, B. Huang, W. Shi, R. Lu, P. Niu, F. Zhan, X. Ma, D. Wang, W. Xu, G. Wu, G. F. Gao, W. Tan, *N. Engl. J. Med.* **2020**, *382*, 727.

[2] World Health Organization (WHO). *Weekly Epidemiological Update on COVID-19*. https://www.who.int/publications/m/item/weekly-epidemiological-update-on-covid-19---22-march-2022

[3] J. Liu, W. Xie, Y. Wang, Y. Xiong, S. Chen, J. Han, Q. Wu, *Int. J. Surg. Lond. Engl.* **2020**, *81*, 1.

[4] J. Koch, Z. M. Uckeley, P. Doldan, M. Stanifer, S. Boulant, P.-Y. Lozach, *EMBO J.* **2021**, *40*, e107821.

[5] A. Pišlar, A. Mitrović, J. Sabotič, U. Pečar Fonović, M. Perišić Nanut, T. Jakoš, E. Senjor, J. Kos, *PLoS Pathog.* **2020**, *16*, e1009013.

[6] T. Tang, J. A. Jaimes, M. K. Bidon, M. R. Straus, S. Daniel, G. R. Whittaker, *ACS Infect. Dis.* **2021**, *7*, 264.

[7] R. Wang, J. Chen, Y. Hozumi, C. Yin, G.-W. Wei, *ACS Infect. Dis.* **2022**, *8*, 546.

[8] T. S. Kim, C. Heinlein, R. C. Hackman, P. S. Nelson, *Mol. Cell Biol.* **2006**, *26*, 965.

[9] B. A. Schuler, A. C. Habermann, E. J. Plosa, C. J. Taylor, C. Jetter, N. M. Negretti, M. E. Kapp, J. T. Benjamin, P. Gulleman, D. S. Nichols, L. Z. Braunstein, A. Hackett, M. Koval, S. H. Guttentag, T. S. Blackwell, S. A. Webber, N. E. Banovich, J. A. Kropski, J. M. Sucre, *J. Clin. Invest.* **2021**, *131*, 140766.

[10] A. K. Clift, C. A. C. Coupland, R. H. Keogh, H. Hemingway, J. Hippisley-Cox, *Ann. Intern. Med.* **2021**, *174*, 572.

[11] B. J. Fraser, S. Beldar, A. Seitova, A. Hutchinson, D. Mannar, Y. Li, D. Kwon, R. Tan, R. P. Wilson, K. Leopold, S. Subramaniam, L. Halabelian, C. H. Arrowsmith, F. Bénard, **2021**, 2021.06.23.449282.

[12] M. Hoffmann, H. Kleine-Weber, S. Schroeder, N. Krüger, T. Herrler, S. Erichsen, T. S. Schiergens, G. Herrler, N.-H. Wu,

[13] A. Nitsche, M. A. Müller, C. Drosten, S. Pöhlmann, *Cell* **2020**, *181*, 271.

[13] T. Hempel, L. Raich, S. Olsson, N. P. Azouz, A. M. Klingler, M. Hoffmann, S. Pöhlmann, M. E. Rothenberg, F. Noé, *Chem. Sci.* **2021**, *12*, 983.

[14] J. D. Gunst, N. B. Staerke, M. H. Pahus, L. H. Kristensen, J. Bodilsen, N. Lohse, L. S. Dalgaard, D. Brønnum, O. Fröbert, B. Hønge, I. S. Johansen, I. Monrad, C. Erikstrup, R. Rosendal, E. Vilstrup, T. Mariager, D. G. Bove, R. Offersen, S. Shakar, S. Cajander, N. P. Jørgensen, S. S. Sritharan, P. Breining, S. Jespersen, K. L. Mortensen, M. L. Jensen, L. Kolte, G. S. Frattari, C. S. Larsen, M. Storgaard, L. P. Nielsen, E. A. Sædder, L. J. Østergaard, H. T. T. Ngo, M. H. Jensen, J. F. Højen, M. Kjolby, O. S. Søgaard, *EClinicalMedicine* **2021**, *35*, 100849.

[15] S. V. Zhuravel, O. K. Khmelnitskiy, O. O. Burlaka, A. I. Gritsan, B. M. Goloshchekin, S. Kim, K. Y. Hong, *EClinicalMedicine* **2021**, *41*, 101169.

[16] I. Midgley, A. J. Hood, P. Proctor, L. F. Chasseaud, S. R. Irons, K. N. Cheng, C. J. Brindley, R. Bonn, *Xenobiotica Fate Foreign Compd. Biol. Syst* **1994**, *24*, 79.

[17] S. Tsukagoshi, *Gan to Kagaku Ryoho* **2000**, *27*, 767.

[18] C. El Amri, *Adv. Exp. Med. Biol.* **2021**, *1304*, 215.

[19] A. F. A. Moumbock, J. Li, P. Mishra, M. Gao, S. Günther, *Comput. Struct. Biotechnol. J.* **2019**, *17*, 1367.

[20] D. Toledo Warshaviak, G. Golan, K. W. Borrelli, K. Zhu, O. Kalid, *J. Chem. Inf. Model.* **2014**, *54*, 1941.

[21] M. Gao, A. F. A. Moumbock, A. Qaseem, Q. Xu, S. Günther, *Nucleic Acids Res.* **2022**, *50*, D445.

[22] V. Martichonok, J. B. Jones, *Bioorg. Med. Chem.* **1997**, *5*, 679.

[23] S. L. Webb, A. J. Sanders, M. D. Mason, W. G. Jiang, *Front. Biosci. Landmark Ed.* **2011**, *16*, 539.

[24] H. T. T. Tran, M. Gigl, N. P. K. Le, C. Dawid, E. Lamy, *Pharm. Basel Switz.* **2021**, *14*, 1055.

[25] Y. J. Sun, G. Velez, D. E. Parsons, K. Li, M. E. Ortiz, S. Sharma, P. B. McCray, A. G. Bassuk, V. B. Mahajan, *J. Clin. Invest.* **2021**, *131*, 147973.

[26] C. T. Pager, R. E. Dutch, *J. Virol.* **2005**, *79*, 12714.

[27] European Chemicals Agency (ECHA). C&L Inventory. https://echa.europa.eu/information-on-chemicals/cl-inventory-database/-/discli/details/95785

[28] X. Hu, C. Z. Chen, M. Xu, Z. Hu, H. Guo, Z. Itkin, P. Shinn, P. Ivin, M. Leek, T. J. Liang, M. Shen, W. Zheng, M. D. Hall, *ACS Med. Chem. Lett.* **2021**, *12*, 1267.

[29] H. M. Berman, J. Westbrook, Z. Feng, G. Gilliland, T. N. Bhat, H. Weissig, I. N. Shindyalov, P. E. Bourne, *Nucleic Acids Res.* **2000**, *28*, 235.

[30] G. M. Sastry, M. Adzhigirey, T. Day, R. Annabhimoju, W. Sherman, *J. Comput. Aided Mol. Des.* **2013**, *27*, 221.

[31] C. Lu, C. Wu, D. Ghoreishi, W. Chen, L. Wang, W. Damm, G. A. Ross, M. K. Dahlgren, E. Russell, C. D. Von Bargen, R. Abel, R. A. Friesner, E. D. Harder, *J. Chem. Theory Comput.* **2021**, *17*, 4291.

SUPPORTING INFORMATION

Additional supporting information can be found online in the Supporting Information section at the end of this article.